A&A 601, A35 (2017)
DOI: 10.1051/0004-6361/201629704

Astronomy & Astrophysics

High-fidelity VLA imaging of the radio structure of 3C 273⋆

R. A. Perley[1] and K. Meisenheimer[2]

[1] National Radio Astronomy Observatory, Socorro, NM 87801, USA
e-mail: rperley@nrao.edu
[2] Max Planck Institüt fur Astronomie, 69117 Heidelberg, Germany

Received 12 September 2016 / Accepted 15 December 2016

ABSTRACT

Context. 3C 273, the nearest bright quasar, comprises a strong nuclear core and a bright, one-sided jet extending ∼23 arcsec to the SW. The source has been the subject of imaging campaigns in all wavebands. Extensive observations of this source have been made with the Very Large Array and other telescopes as part of a campaign to understand the jet emission mechanisms. Partial results from the VLA radio campaign have been published, but to date, the complete set of VLA imaging results has not been made available.
Aims. We have utilized the VLA to determine the radio structure of 3C 273 in Stokes I, Q, and U, over the widest possible frequency and resolution range.
Methods. The VLA observed the source in all four of its configurations, and with all eight of its frequency bands, spanning 73.8 MHz to 43 GHz. The data were taken in a pseudo-spectral line mode to minimize the VLA's correlator errors, and were fully calibrated with subsequent self-calibration techniques to maximise image fidelity.
Results. Images in Stokes parameters I, Q, and U, spanning a resolution range from 6 arcsec to 88 milliarcsec are presented. Spectral index images, showing the evolution of the jet component are shown. Polarimetry demonstrates the direction of the magnetic fields responsible for the emission, and rotation measure maps show the RM to be very small with no discernible trend along or across the jet. This paper presents a small subset of these images to demonstrate the major characteristics of the source emission. A library of 294 images has been made available at the CDS.

Key words. radio continuum: galaxies – galaxies: jets – quasars: general

1. Introduction

3C 273 (J1229+0203), the first identified quasar (Schmidt 1963), is one of the closest and most luminous of all quasars. Imaging of this source shows that at all wavebands, 3C 273 comprises a bright, flat-spectrum nucleus with highly variable flux density, and a one-sided, highly polarized, narrow jet extending ∼23 arcsec to the SW, at PA −138°, from the nucleus. Since its discovery, and due to its relative proximity (z = 0.158, so 1 arcsec ∼ 2.7 kpc)[1] and angular size, 3C 273 has been observed by a wide range of instruments from long-wavelength radio through X-ray.

The results from radio observations of 3C 273 by the Very Large Array (VLA) and by the Multi-Element Radio-Linked Interferometer (MERLIN), taken prior to 1985, were reported by Conway et al. (1993). Since then, 3C 273 has been the target of an extensive and comprehensive observational campaign spanning many wavebands and utilizing many telescopes from 1995 through 2005. Key results from this campaign are to be found in Jester et al. (2005), and references within, which present results from observations made with the Very Large Array from 8 through 43 GHz, along with *Hubble* Space Telescope (HST) observations from the near-ultraviolet through near-infrared. However, the radio images shown in this paper are a small selection of those available from the suite of VLA observations of this source.

The purpose of this paper is to present an overview of the key results from all the VLA imaging of 3C 273, utilizing the data taken between 1987 and 1999. All the images resulting from these projects are now publicly available, through links given later in this paper.

2. Observations

The results presented here are from three separate observational campaigns utilizing the Very Large Array[2], each with different goals. The first, taken in 1987, 1991 and 1999 under project codes AP134, AB608, and AB916 was intended to search for changes in the structure of the radio jet over a 12-yr span of time. The second, in 1995 through 1997, under project codes AR334 and AR371, were part of a full spectral and resolution coverage study of the jet emission properties spanning six VLA frequency bands. Neither of these projects included observations from the low frequency bands, at 73.8 and 327 MHz. The results included in this paper from these bands are taken from project AK461, whose goal was to demonstrate the imaging capability of the VLA at low frequencies by observing a selection of 3C sources, including 3C 273.

The observing details for all these projects are given in Table 1. To minimize the baseline-based errors ("closure errors") which limit image fidelity for very bright sources such as 3C 273, we employed the spectral line mode "1A", providing 64 channels in a single correlation over 12.5 MHz bandwdth, or "PA"

⋆ The image library (FITS files) is only available at the CDS via anonymous ftp to cdsarc.u-strasbg.fr (130.79.128.5) or via http://cdsarc.u-strasbg.fr/viz-bin/qcat?J/A+A/601/A35

[1] H_0 = 70, Ω_M = 0.286, Ω_v = 0.714.

[2] The National Radio Astronomy Observatory is a facility of the National Science Foundation operated under cooperative agreement by Associated Universities, Inc.

Table 1. VLA observing log.

Project	Date	Conf.	Bands[a]	Dur. (h)
AP134	07 Sep. 1987	A	*C*, *U*	12
AP134	10 Sep. 1987	A	*C*, *U*	12
AB608	04 Jul. 1991	A	*C*, *U*	12
AB608	14 Jul. 1991	A	*C*, *U*	12
AR334	09 Jul. 1995	A	*L*, *C*, *X*, *U*, *K*, *Q*	12
AR334	13 Oct. 1995	B	*L*, *C*, *X*, *U*, *K*, *Q*	12
AR334	01 Mar. 1996	C	*L*, *C*, *X*, *U*, *K*, *Q*	12
AR371	08 Nov. 1997	D	*L*, *C*, *X*, *U*, *K*, *Q*	6
AK461	07 Mar. 1998	A	4, *P*	24
AB916	19 Jun. 1999	A	*C*, *U*	10

Notes. [(a)] 4: 73.8 MHz, *P*: 327 MHz, *L*: 1365 MHz, *C*: 4885 MHz, *X*: 8415 MHz, *U*: 14965 MHz, *K*: 22485 MHz, *Q*: 43315 MHz.

with a bandwidth of 12.5 MHz, providing all four complex correlations with 16 channels each. The low frequency observations were taken in a dual frequency mode, providing only the parallel hand correlations in spectral line mode "4", with 3.125 MHz bandwidth at 327 MHz, and 1.56 MHz bandwidth at 73.8 MHz.

Because 3C 273 is a very strong radio source with a nuclear core suitable for calibration, a special calibration regimen was adopted. At the lower frequencies (1365 MHz, 4885 MHz, and 8415 MHz), where the jet emission is significant and the array resolution lower, phase and amplitude calibrations were accomplished with the nearby unresolved source J1150−0023. At the higher frequency bands (14 965 MHz, 22 485 MHz, and 43 315 MHz), this secondary calibrator was not necessary, and the nuclear component of 3C 273 itself provided the calibration.

The observations for projects AR334 and AR371 were arranged on an hourly cycle, within which the first 17 min were used for the observations at the lowest three frequencies (including b the calibrator), followed by 10 min of 14 965 MHz, 12 min at 22 485 MHz, and 15 min at 43 315 MHz. This variation of duration with frequency was done to offset the loss of sensitivity at the higher frequency bands. Referenced pointing, a technique which determines the local pointing offsets, was done utilizing 3C 273 at *X*-band, with the corrections applied to the subsequent observations at these higher frequencies.

The VLA's 40–50 GHz system (*Q*-band) was being implemented during this program, with the result that only 9, 11, 13, and 13 antennas were outfitted for the A, B, C, and D configuration observations, respectively. As this system was in its early stages, and because we did not expect to be able to accomplish detailed structure studies with the incomplete system, we observed only every other hour at this band.

The flux density scale was set through an observation of 3C 286, the VLA's primary flux density calibrator, at the end of each observing run. The values used have been adjusted to the new scale of Perley & Butler (2017), which are based on the Baars et al. (1977) for the frequencies below 2 GHz, and on quantitative emission models of Mars for the high frequencies. This new scale is an extension to lower frequencies of the Perley & Butler (2013a) scale. The values utilized are shown in Table 2.

Calibration of the data was done using the `AIPS` software package, using the following procedure:

1. Quick inspection of the amplitude data was used to remove obviously bad data from "dead' antennas.
2. The bandpass functions for the polarizations observed were determined using 3C 273 itself, using BPASS.

Table 2. Flux density of 3C 286 used for this work.

Band	Freq. MHz	Flux density Jy
P	327	26.3
L	1365	15.2
C	4885	7.29
X	8415	5.07
U	14 915	3.38
K	22 485	2.51
Q	43 315	1.54

3. The spectral channel data were corrected by the bandpass, and collapsed to a single "pseudo-continuum" channel, using SPLAT. The result is a single-frequency, multi-source database, similar to what the continuum system provides, but with much reduced baseline-dependent ("closure") errors.
4. As 3C 286 is partially resolved to most configurations at all frequencies, our observations of this source were used to construct a source model whose brightness scale was adjusted to give the correct total flux density given in Table 2.
5. These models of 3C 286 were then used by CALIB to determine the antenna gains, and to derive the flux density of the calibration source J1150−0023 at *L*, *C*, and *X* bands. For the higher frequencies, the flux density of 3C 273 was derived directly, using the longer spacings for which the nuclear core is cleanly separable from the jet emission.
6. For the higher frequency observations, the elevation dependency of the antenna gains was determined by ELINT, with the resulting dependencies applied to the data from all sources.
7. The time-variable complex gains (amplitude and phase) were then derived, using J1150−003 for *L*, *C*, and *X* bands, and using 3C 273 itself for *U*, *K*, and *Q* bands via CALIB, and applied using CLCAL.
8. The polarization calibration program PCAL was used to determine the antenna polarization, using the calibrator source J1150−003 for the lower three frequency bands, and 3C 273 itself for the three highest frequency bands..
9. The RCP – LCP phase difference was determined by observation of the plane of polarized flux for 3C 286, using the widely accepted value of 33°, and applied to the data using CLCOR. The small position angle corrections noted by Perley & Butler (2013b) were not applied.
10. The data were then split out by source into individual files, applying all gains, for subsequent self-calibration and imaging, using AIPS program SPLIT.

Calibration of the 73.8 and 327.5 MHz data followed a similar procedure (minus the polarization calibration stage), except that at 327.5 MHz, the phase calibration was based on the global average of observations of 3C 286, 3C 147, 3C 48, and 3C 138, while at 73.8 MHz, only Cygnus A was used for amplitude calibration, using the Baars et al. (1977) values of 17 130 Jy.

All subsequent calibration was done on a single-source basis, separately for each frequency and configuration, utilizing well-established methodologies of self-calibration. For sources like 3C 273, comprising simple structures with sharp brightness gradients, these procedures are especially effective. Although the use of the spectral line correlator modes reduced the "closure"[3] errors to very small values – typically to 0.1% and 0.05 degrees

[3] These are defined as baseline-based errors which cannot be factored out by antenna.

Table 3. Variability in flux density and polarization of the nucleus of 3C 273, for A, B, C and D configurations.

Date		*L*	*C*	*X*	*U*	*K*	*Q*
		1365	4885	8415	14 965	22 345	43 340
09	*I* (Jy)	33.3	35.5	32.3	27.8	22.9	20.2
Jul.	χ	−27	−23	−26	−21	−35	−19
1995	%	0.9	3.0	3.4	5.6	4.3	4.6
13	*I* (Jy)	32.8	35.6	30.0	24.3	19.8	16.1
Oct.	χ	−28	−21	−26	−24	−29	−32
1995	%	1.0	3.1	3.0	5.8	6.0	3.4
01	*I* (Jy)	31.7	36.1	26.9	22.3	24.3	30.8
Mar.	χ	−34	−23	−26	−30	−40	−40
1996	%	0.8	3.0	4.2	6.1	4.1	2.9
08	*I* (Jy)		29.6	26.7	31.5	35.6	37.7
Nov.	χ		−23	−26	−33	−36	−38
1997	%		3.1	4.7	3.2	2.8	2.1

Notes. Estimated accuracies: in flux density ∼5%; in position angle ∼5 degrees; in fractional polarization 0.5%.

– a baseline-based calibration step, using the AIPS program BLCAL, was done for some of the frequency/configuration databases, if the characteristic sign of the effect of these errors was seen in any map[4].

Self-calibration was done for each frequency and configuration separately. Following this, the databases from different configurations were combined to permit imaging over a very wide range of spatial scales, and to provide the best dynamic range and sensitivity at each frequency. Because the nuclear source of 3C 273 is variable, and the observations for AR334 and AR371 were taken over a 2.5 yr timescale, the flux density of the nuclear emission (in all three Stokes' parameters) had to be adjusted to a common value before combining the four configurations' data. This was done using the AIPS program UVMOD, using the A-configuration values as the reference. The flux densities and polarizations of the nucleus, as a function of time and frequency, are given in Table 3. The values listed were derived from analysis of the images, as described in the following section. There are no values listed at *L*-band in D-configuration, as the resolution is too low to enable a trusworthy separation of the nucleus from the extended emission. Errors in Stokes' *I* are conservatively estimated to be ∼5% at the five lowest frequency bands, and ∼10% at *Q*-band. Errors in the fractional polarization and position angles are estimated to be ∼0.5% and ∼5 degrees, respectively. The doubling of the core flux density at *Q*-band between October 1995 and November 1996, with proportionally lesser increases at *K* and *U* bands, indicates a new outburst whose spectral evolution follows the synchrotron bubble model of van der Laan (1966).

3. Imaging

We present here images of the structure of 3C 273, with resolutions chosen to highlight the major structural components of the source. In the following figures, the bottom contour level is set to approximately the 3σ brightness level.

Imaging of the source was done in Stokes parameters *I*, *Q*, and *U*, using the AIPS program "IMAGR". Primary beam attenuation was corrected for at all bands via use of the program "PBCOR", utilizing the coefficients contained within.

[4] For a source located near the equatorial plane, like 3C 273, these errors are manifested as a vertical disturbance up the center of the image.

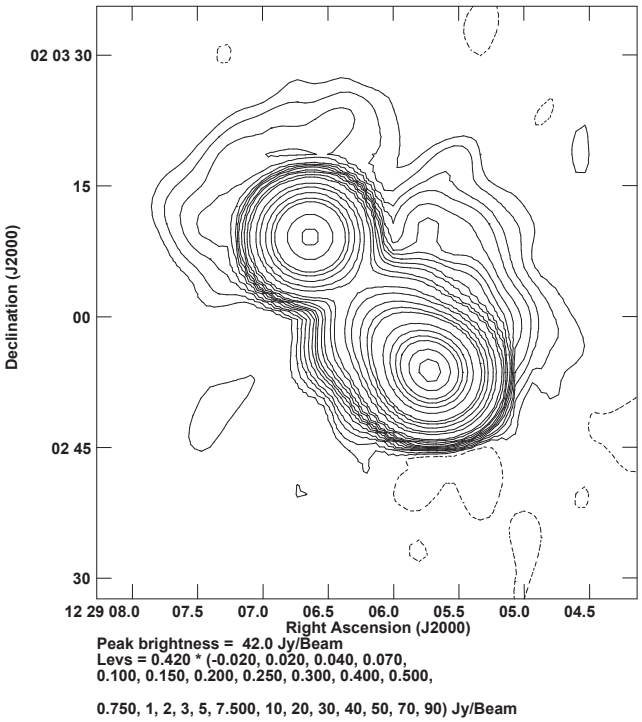

Fig. 1. 3C 273 at 327 MHz, with 6 arcsec resolution. The extended halo emission, slightly offset from the bright emission, is clearly visible.

The flux densities of the jet and halo were determined via "TVSTAT", while the flux density of the nucleus was determined via "JMFIT", or through examination of the clean components.

Low resolution images of the source at ∼5 arcsec resolution at *P*, *L*, and *C* bands are shown in Figs. 1 through 3. These show the presence of a previously unknown diffuse component of emission. This emission is of approximate extent 30 by 45 arcsec, centered approximately 10 arcsec (or 27 kpc) to the north of the brighter core and jet emission, and aligned with the jet axis. Figure 1 shows the structure at 327 MHz, with 6 arcsec resolution, Figs. 2 and 3 show the structure at 1365 MHz and 4885 MHz with 4 arcsec resolution. Imaging at 1465 MHz with 15 arcsec resolution shows no other extended emission to our brightness sensitivity level of ∼0.6 mJy/beam.

The extended emission to the north-east of the core is unpolarized to a level of ∼0.1 mJy/beam at *L* and *C* bands, implying a maximum fractional polarization of <5%. The brighter extended emission, immediately to the north of the jet (most clearly shown in Fig. 2) shows a marginal detection of polarized flux at *L*-band, with a maximum fraction of ∼10%.

The images made at 4 arcsec resolution clearly show the halo at the lowest three frequencies (327, 1465, and 4885 MHz). The differences in the halo brightness distribution apparent between Figs. 1 and 2 should not be interpreted as evidence for significant spectral variations, as the process of self-calibration, and in particular, that of baseline-based calibration, are likely to have generated these variations. We do, however, believe the detection of the halo to be secure.

The three major components – core, jet, and halo, can be separated by suitable integration of the image brightnesses, with the resulting total flux densities for these components given in Table 4. This extended halo of emission – unknown before these observations – may represent the lobes of a low-luminosity "FR1" radio source. In this interpretation, the nuclear core and

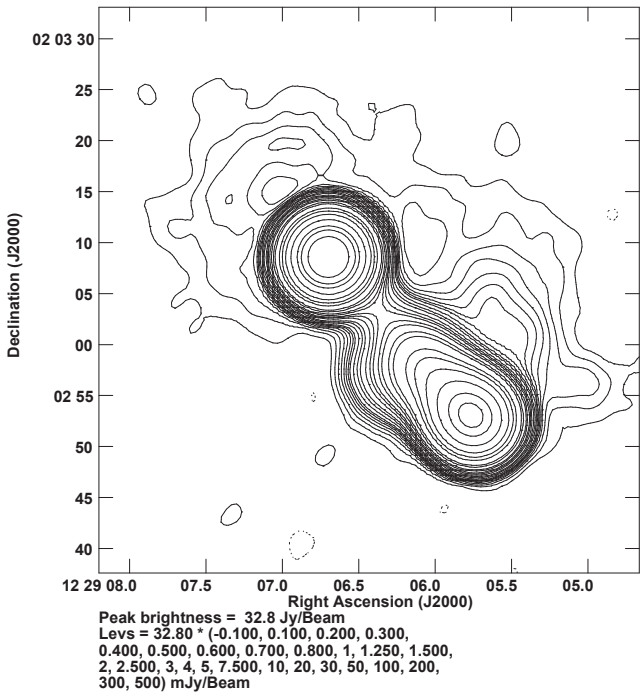

Fig. 2. 3C 273 at 1365 MHz, with 4 arcsec resolution. The extent of the halo is similar to that at 327 MHz, although the details of the emission differ somewhat.

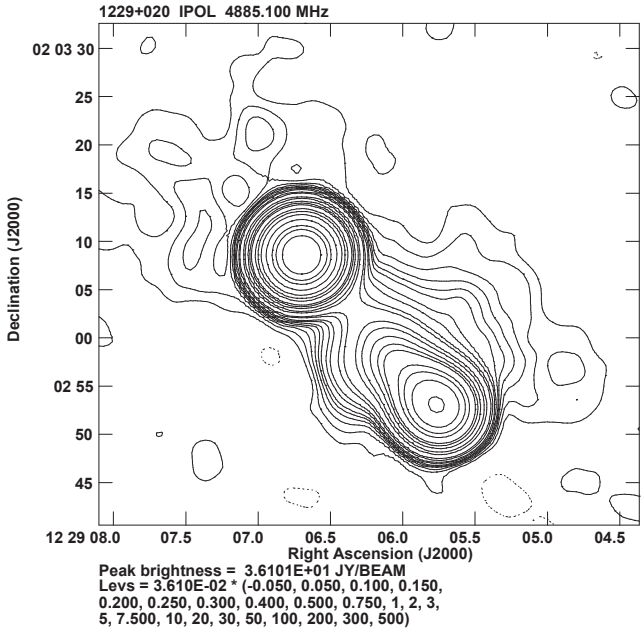

Fig. 3. 3C 273 at 4885 MHz, with 4 arcsec resolution. The overall extent of the diffuse emission is similar to that at 327 and 1365 MHz, but the details differ, most likely due to variations introduced by the calibration and imaging process.

the one-sided jet represent Doppler-brightened emission from a relativistic flow aligned close to the line of sight.

It will be noted from Figs. 1 and 2 that there is a modest "bulge" of emission on the eastern side of the source, about midway down the jet. This structure, which was previously seen by imaging with MERLIN, (Conway et al. 1993) is more clearly shown at 2 arcsec resolution in Fig. 4. In Fig. 5 we show the linear polarization of the emission at a 2 arcsec resolution at 1365 MHz.

Table 4. Core and extended flux densities for 3C 273 (July 1995).

Frequency MHz	Core Jy	Jet Jy	Halo Jy
73.8	9.1	151.5	?
327.5	13.3	55.4	0.84
1365	33.3	17.5	0.30
4885	35.5	5.65	0.15
8415	32.3	3.40	0.04

Notes. Errors in core flux density ~5%, in jet flux density ~10%, in the halo flux density ~30%.

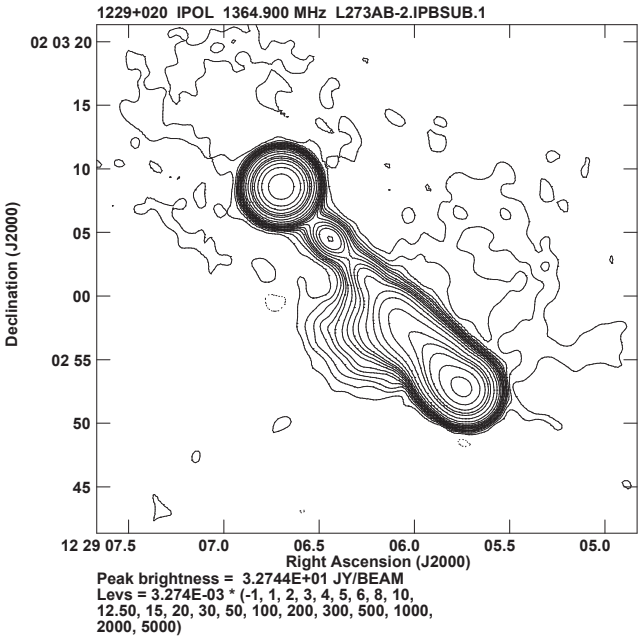

Fig. 4. 3C 273 at 1365 MHz, with 2 arcsec resolution. The inner and outer jets are now visible, while the faint halo is now nearly resolved out. The brighter extension to the SE of the outer jet is clearly visible.

Increasing the resolution by another factor of two resolves out the extended emission completely, and reveals detailed structures of the jet emission itself. Figure 6 shows the emission with 1 arcsec resolution at 14 965 MHz. Notable here is the presence of a bright, straight, apparently unresolved inner jet, extending halfway between the nuclear core and well-resolved outer jet.

The inner jet has previously been detected in observations by MERLIN (Davis et al. 1985) and the VLA (Conway et al. 1993), but with poorer sensitivity than the results shown here. Optical emission from this inner jet has been reported from HST observations by Martel et al. (2003).

Figure 7 shows the polarization at 8415 MHz with 1 arcsec resolution. The inner jet polarization is quite low, typically 5 to 10%, with the *B*-field direction oriented along the jet. The outer jet shows considerable variation in polarization structure, with a high degree of polarization (~30%) along the edges, and much lower values throughout the center.

The structures of the inner and outer jets are strikingly different, as illustrated in a very deep image, taken at 4866 MHz, with 0.4 arcsec resolution, shown in Fig. 8. Some important features of the jet structure seen in the figure are noted here:

- The inner jet is nearly straight, and is transversly unresolved.
- There are three elongated enhancements in brighness along this inner portion, separated by 5 arcsec.

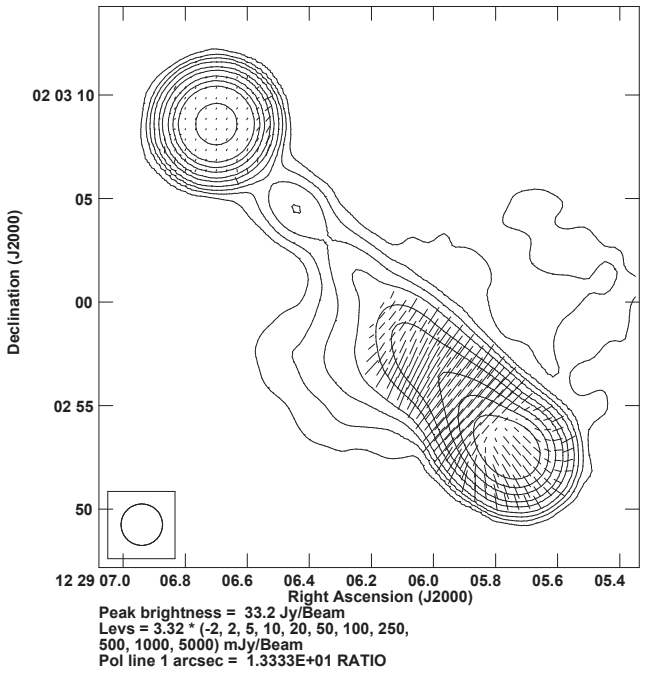

Fig. 5. Polarization of 3C 273 at 1365 MHz with 2 arcsec resolution. The plotted *E*-vectors show the orientation of the plane of linear polarization, their lengths are proportional to the degree of polarization. The observed pattern shows that the projected magnetic field is along the jet, and wraps around the end. This pattern, with the *B*-field aligned with the edges of the emission, is the general rule for synchrotron-emitting extragalactic radio sources. The extended emission to the SE of the jet is polarized at a level at or less than 15%.

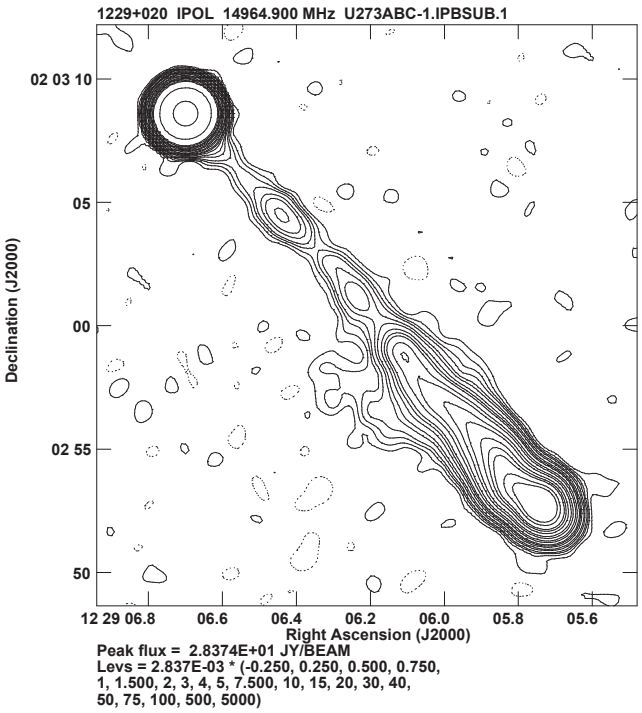

Fig. 6. 3C 273 at 14 965 MHz, with 1 arcsec resolution. The extended emission is nearly resolved out, while details of the inner jet are becoming clear.

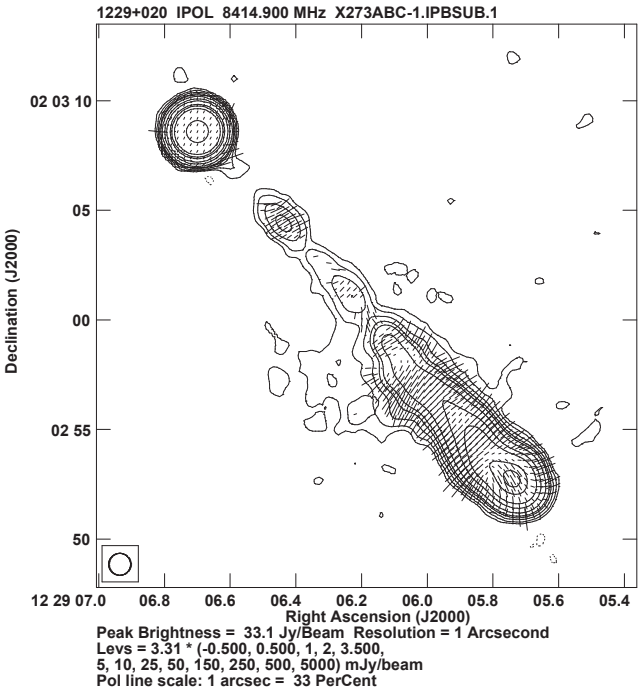

Fig. 7. Polarization of 3C 273 at 8415 MHz, with 1 arcsec resolution. The projected magnetic field orientation is orthogonal to these plotted *E*-vectors, and accurately follows the brightness isocontours.

- These three elongated enhancements are not perfectly colinear – the outer two are tilted, in opposite directions, by about 5 degrees with respect to the jet axis. The innermost enhancement is perfectly colinear with the brightest hotspot near the end of the outer jet.
- An emerging, unresolved, knot of emission is seen 550 milliarcsec outside the nuclear position. This structure is to be identified with the innermost jets seen on milliarcsecond scales with the VLBA by Zavala & Taylor (2005).
- The inner jet abruptly transitions to a wider (~3 arcsec) outer jet, 12 arcsec from the nucleus.
- The outer jet exhibits considerable variations in structure, including an oscillatory center brightness with 6 arcsec period, and ~1 arcsec amplitude.
- There is a prominent flattened knot of emission 22 arcsec from the nucleus ("H2" in the nomenclature of Jester et al. 2005) oriented transverse to the jet axis. Smoother, lower-brightness emission ("H1" in Jester et al. 2005) is detected for 1.5 arcsec beyond this knot.

The oscillatory behavior of the central spine of emission within the outer jet is more clearly seen with 0.25 arcsec resolution at 14.9 GHz, as shown in Fig. 9.

At 125 milliarcsec resolution, more details of the brighter components of the jet become visible. The innermost jet is clearly visible, as shown in Fig. 10. No polarized flux from this inner jet was detected at this resolution, as the noise level in this region is near 5 mJy/beam – comparable to the jet brightness. The outer jet, at this same resolution, is seen in Fig. 11.

The detailed polarization image at 0.25 arcsec resolution shows a considerably more complex structure than in total intensity, as shown in Fig. 12. The polarization fraction is generally low in the interior regions of the jet, and reaches high values – as high as 55% – along the boundaries. The projected magnetic field accurately follows the total intensity boundaries of the jet. At 0.125 arcsec resolution, the only detectable polarization emission at 14.9 GHz is from the brightest structures associated with the hotspot, as shown in Fig. 13. The degree of

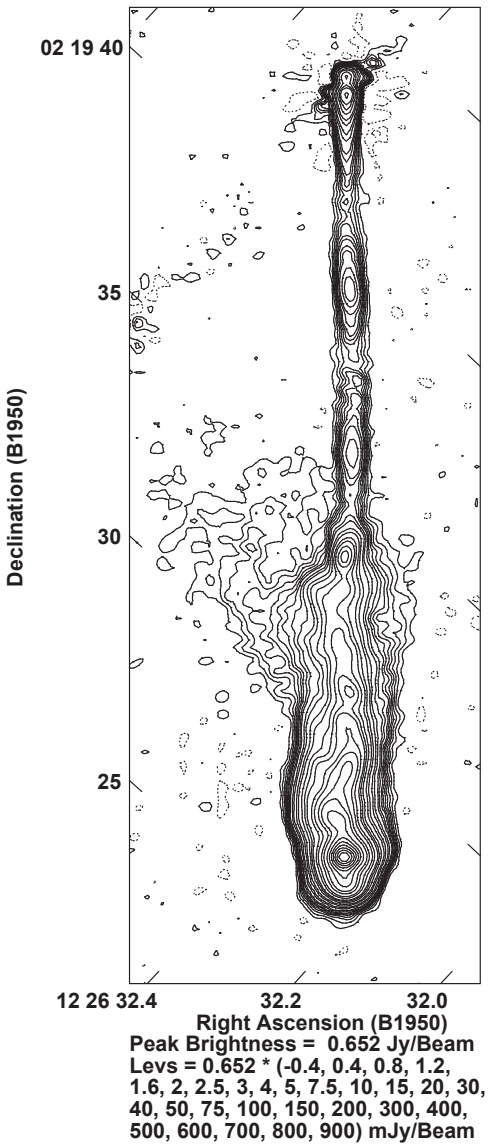

Fig. 8. 3C 273 at 4865 MHz and 0.40 arcsec resolution, rotated CW by 42.36 degrees. The unresolved nuclear component has been removed, leaving a 30 mJy residual at the top to mark the nuclear position. Notable here is the high brightness of the inner jet, which is transversely unresolved.

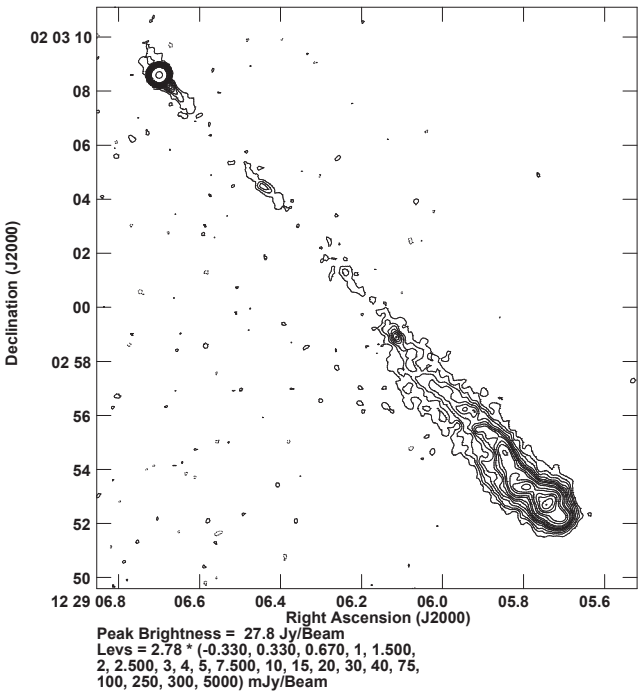

Fig. 9. 3C 273 at 14 965 MHz, with 0.25 arcsec resolution. The oscillatory structure of the outer jet is now more clearly evident.

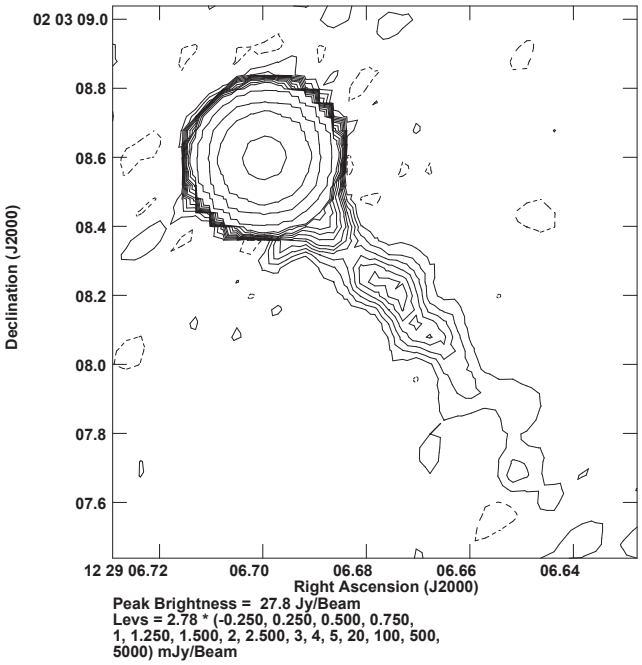

Fig. 10. The innermost jet, as seen at 14 965 MHz, with 125 milliarcsec resolution. The "protrusion" in emission 0.20 arcsec to the SW of the nucleus is the end of the milliarcsecond-scale jet.

polarizaton in general remains relatively low in these bright areas – typically 10%, but reaches ~40% at the bright hotspot, with a magnetic field orientation perpendicular to the jet main axis.

Concluding this section on the structure of the jet, we show our highest resolution image – 88 milliarcsec at 22 345 MHz – in Fig. 14. The bright hotspot is now fully resolved. No polarized emission is detected, due to insufficient surface brightness sensitivity. A limit in the fractional polarization of 10% on the compact bright knots, and 30% on the extended emission is set.

4. Spectral index

Spectral index images are utilized for identifying areas of either active particle acceleration or dominant synchrotron losses. When combined with an estimate of the magnetic field strength, ages of the relativistic electron population since last acceleration, and thus source expansion velocities can be inferred. Our comprehensive imaging campaign permits spectral index images of the jet over a wide range of resolutions and frequencies.

We show, in Fig. 15 a four-panel spectral index image[5] at 2.0 arcsec resolution, spanning 1.365 through 22.3 GHz. These images were generated using the AIPS task "COMB", from images generated by IMAGR, using a common cellsize and deconvolution restoring beam. Registration of the images was set

[5] Defined as $\alpha = (\log(B_{\nu 1}) - \log(B_{\nu 2}))/(\log(\nu 2) - \log(\nu 1))$.

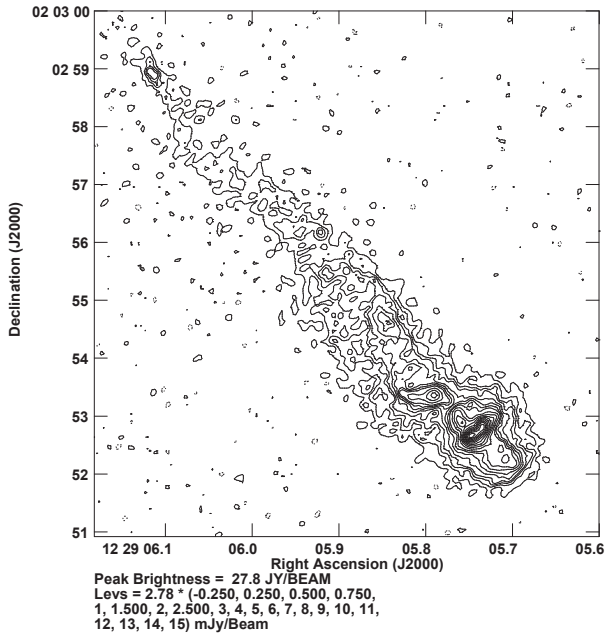

Fig. 11. The brightest portions of the outer jet at 0.125 arcsec resolution, showing the brightest hotspot, and the oscillatory ridge leading to it.

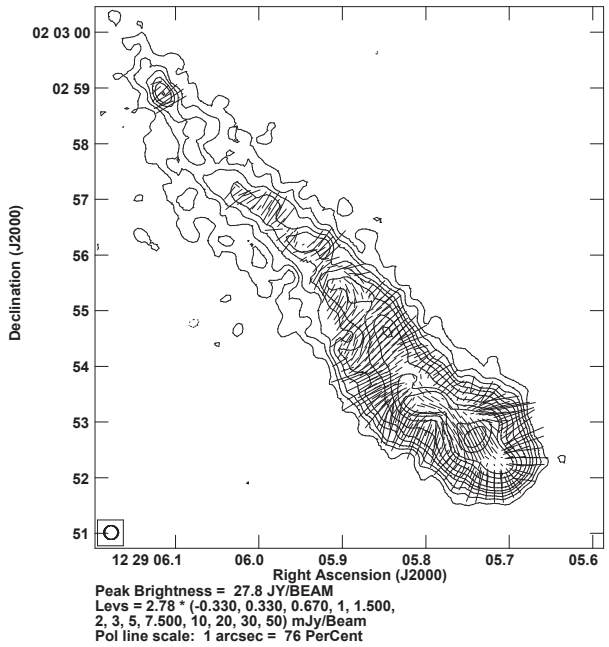

Fig. 12. The polarization structure of the outer jet at 14965 MHz, with 0.25 arcsec resolution. The length of the vectors indicates the fractional linear polarization. Their orientation is perpendicular to the projected jet magnetic field.

through the self-calibration process, which always started with the nucleus fixed to the phase-tracking center. The blanking in COMB was set to an SNR of 10:1 in spectral index.

Figure 15 shows that the inner jet has a spectral index near 0.65, and that the outer jet has a uniform spectral index near 0.85. There is a notable steepening of the radio spectral index in the vicinity of the brightest hotspot, to 1.0, between 14 965 and 22 485 MHz. The spectral index in the hotspot vicinity at higher frequencies continues to steepen, reaching approximately $\alpha_{23345}^{43340} \sim 1.4$ between 23.3 and 43.3 GHz.

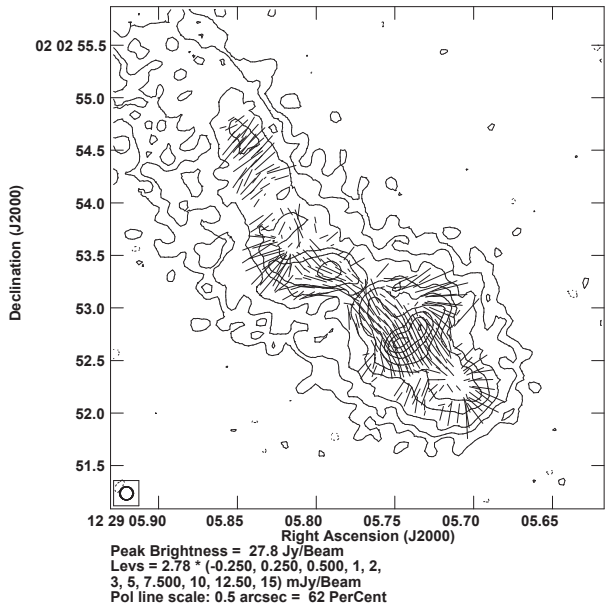

Fig. 13. The polarization structure of the outer jet at 14 965 MHz, with 0.125 arcsec resolution. The polarized emission from the more extended regions of the jet is not visible due to insufficient sensitivity.

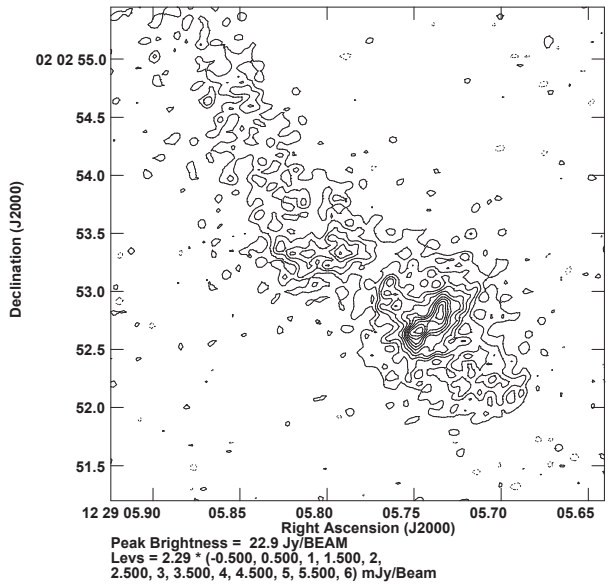

Fig. 14. The structure of the brightest hotspot at 22 345 MHz, with 0.088 arcsec resolution. The hotspot is now almost completely resolved out, indicating there are no physical structures less than ~300 pc in size.

The high frequency steepening of the spectrum is not a property of the brightest hotspot only, however, as is made clear in Fig. 16, showing the spectral index images between *X* and *K* bands at 0.25 arcsec resolution.

The spectral index of the low-brightness extended emission to the north and east shown in Figs. 1 through 3 could not be reliably determined, as the brightnesses are too low to permit sufficiently accurate images. However, the integrated fluxes shown in Table 4 can be used to provide a rough measure of $\alpha \sim 0.6$. This value is appropriate for the average over the entire halo.

The interpretation of these spectral trends is beyond the scope of this paper. We refer the reader to the thorough

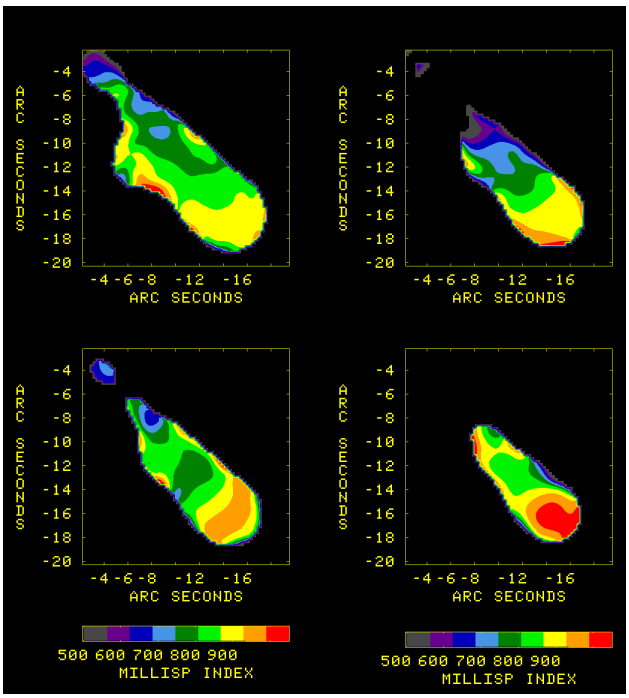

Fig. 15. A four-panel figure showing the change in spectral index through the centimeter radio band, at 2.0 arcsec resolution. *Upper left*: α^{4885}_{1365}; *upper right*: α^{8415}_{4885}; *lower left*: α^{14965}_{8415}; *lower right*: α^{22345}_{14965}. These show the dramatic high frequency steepening of the spectrum in the region of the bright radio hot spot. The images are blanked when the errors in spectral index are greater than 0.1.

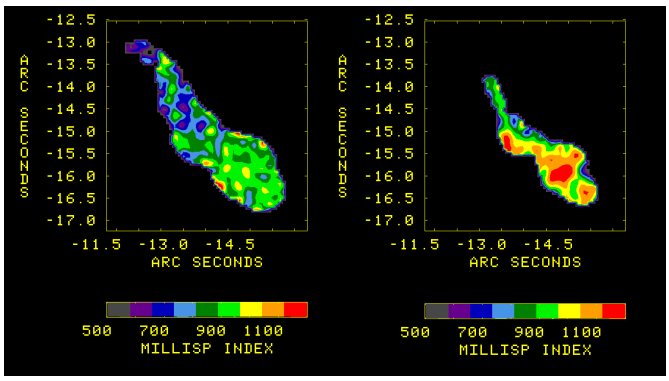

Fig. 16. A two-panel figure showing the change in spectral index through the centimeter radio band at 0.25 arcsec resolution. *Left*: α^{14965}_{8415}; *right*: α^{22345}_{14965}. These show the dramatic steepening of the spectrum in the region of the brightest radio hot spot "H2" is not confined to the hotspot alone, but extends well beyond, in both directions. The images are blanked when the error is greater than 0.1 in spectral index.

discussion given in Jester et al. (2005), which incorporates observations extending from the radio through the ultraviolet.

5. Rotation measure

Propagation of linearly polarized emission through a magnetized, ionized medium results in a rotation of the observed plane of polarization by $RM\lambda^2$ radians, where

$$RM = \int 0.81 n_e B_{\|} \mathrm{d}s \qquad (1)$$

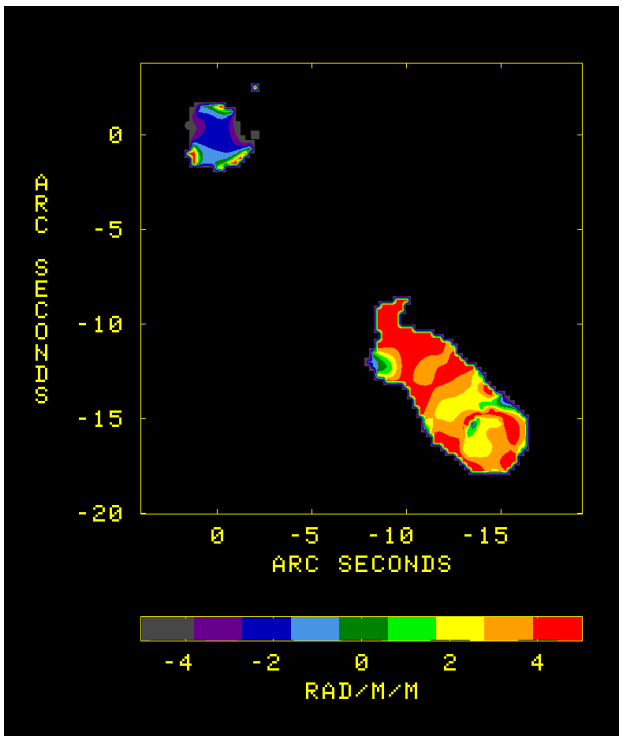

Fig. 17. Rotation measure as determined from the 1365 and 4885 MHz position angle images at 1.4 arcsec resolution. The small-scale variations seen in both the jet and nucleus are artefacts from the noise. The jet has a uniform RM both across and along its axis. The image is blanked when the SNR of the output pixel is less than 5.

is the rotation measure, in units of rad m^{-2}. Here, n_e is the electron density in cm^{-3}, $B_{\|}$ is the longitudinal component of the magnetic field in μG, s is the path length in parsecs, and λ is the wavelength in meters. Measurement of the RM, in combination with knowledge of the ionized gas distribution, provides information on the magnetic fields in the ionized medium.

The polarization postion angle images of 3C 273 allow a determination of the rotation measure, utilizing a pair of position angle images at different frequencies made with the same cell-size and CLEAN restoring beam. Our most sensitive measure is between the lowest pair of frequencies, 1365 and 4885 MHz. Figure 17 shows the RM at 1.4 arcsec resolution. The RM of the entire outer jet is uniform, with mean value 3.7 rad/m^2, with a dispersion of only 1.7 rad/m^2. There is no discernible gradient either across, or along the jet. The RM of the nucleus is slightly less: −2.0 rad/m^2. These very low values suggest there is very little ionized gas in surrounding environment of 3C 273. The sparse frequency coverage does not permit a more detailed analysis (i.e. through use of the "rotation measure synthesis" method of Brentjens and deBruyn 2005). These RM results are similar to those reported by Conway et al. (1993), but there are two significant differences:

- our observations show a small increase in RM of about 1 rad m^{-2} between the bright knot "H2" and the outer jet emission three arcsec upstream, while Conway et al. (1993) claim a small decrease of −0.45 rad m^{-2};
- we see no evidence of the transverse gradient in RM of 0.8 rad m^{-2} claimed by Conway et al. (1993). However, it is to be emphasized that such a small RM results in a change in position angle at λ = 0.2 cm of only 2 degrees – at the limit of detectability in our polarimetry.

The question of the existence of a transverse RM gradient is an important one for jet models – see the discussion by Conway et al. (1993). The issue can only be settled with accurate low-frequency, high resolution polarimetry. Because of its high brightness, angular size, and simple structure, 3C 273 is perhaps the ideal source for such a future study.

6. Image archive

The results shown here are a small fraction of the approximately 500 images available from this project. We have placed 294 of these images, in FITS format, at the CDS. The images are named in a manner which provides sufficient information to identify the content. All files are named thusly:

bb273-rr.type
where

- "bb" is the band or bands utilized for the image;
- "rr" is the resolution of the restoring beam, in arcseconds;
- "type" is the type of image.

There are many possibilities for "type". These include:

- "*I*", "*Q*" or "*U*" denotes the Stokes polarization;
- "Rnnn" indicates the image has been rotated by nnn degrees;
- "SPX.1" denotes spectral index, blanked if the (1σ) error is greater than 0.1;
- "DGPL10" denotes degree of polarization, blanked if the 1σ error is greater than 10%;
- "POLAnn" denotes polarization angle of the electric vector in degrees. When followed by a number, pixels with 1σ error level above nn degrees are blanked;
- "POLC" denotes polarization fraction, corrected for Ricean bias;
- "RM" denotes rotation measure.

All images have been corrected for the primary beam attenuation.

For example, "U273-0.125.I" is a Stokes *I* clean image, with 0.125 arcsec resolution. "UX273-1.4.SPX.1" is a spectral index image between *U* and *X* bands, with 1.4 arcsec resolution, with an error threshold of 0.1 in spectral index. (All pixels with rms error greater than 0.1 are blanked). "U273-1.4.DGPL10" is a fractional polarization image, at *U*-band, with 1.4 arcsec resolution, blanked if the error is more than 10%.

7. Conclusions

The Very Large Array has been utilized to generate high-fidelity radio images of the iconic quasar 3C 273. Major features found by this work include:

- A previously unknown low-brightness steep-spectrum diffuse halo, of extent 30×45 arcsec, primarily on the northern and western sides of the bright nucleus and jet.
- A bright, narrow, nearly straight inner jet, of 12 arcsec length, joining the bright nucleus to the outer jet. The transition in width from the narrow to wider jet is abrupt.
- The inner jet comprising three elongated regions of enhanced brightness, the outer two of which are oppositely tilted by about 5 degrees from the jet axis, suggestive of an oscillatory or sinusoidal underlying structure of period ~5 arcsec.
- The outer jet, of width ~2.5 arcsec, which also comprises an oscillatory structure, with a similar period, but significantly larger amplitude.
- The outer jet is highly linearly polarized, with the polarization fraction reaching 55% along the jet boundaries. The fractional polarization in the central regions of the outer jet is much lower. The projected magnetic field accurately follows the lines of constant brightness, including curling around the leading edge of the jet.
- The inner jet is also highly polarized, with the magnetic field lines oriented along the jet axis.
- The bright radio hotspot "H2" is fully resolved with ~0.09 arcsec (300 pc) resolution.
- The spectrum of the outermost regions of the radio jet sharply steepens above 5 GHz. The inner jet's spectrum is flatter than that of the outer jet.
- The rotation measure of the jet is uniform, with no visible gradient either across or along the jet.

Despite the detailed information on the structure of this source provided by this work, much remains uncertain, or poorly determined. We note, in particular:

- The structure of the newly-discovered halo is very uncertain. While we are confident in the existence of this emission, the differences in structures suggested by comparison of Figs. 1 to 3 are unlikely to be real.
- The current images are noise limited at all the higher frequencies, particularly in polarization. Hence, details of the jet structure and polarization at high frequencies and at high resolution are poorly determined.
- The polarization of the inner jet is only approximately known, since the high-fidelity data taken in 1987 and 1991 were in a single-polarization mode.
- The important issue of rotation measure gradients remains unresolved, but addressable by low frequency, high-resolution polarimetry.

The recent upgrade of the Very Large Array can address all these, and other issues. With the dramatic increase in bandwidth, improved receiver sensitivities, and especially with the implementation of a much more powerful correlator, much superior imaging of this source – and other such sources – is easily in range.

Acknowledgements. R.A.P. is pleased to acknowledge the generosity and hospitality of the Max-Planck Institut fur Astronomie, and in particular that of Hermann-Josef Röser, during his many visits to Heidelberg, where most of this work was done. R.A.P. also thanks Jean Eilek and Brian Punsly for helpful comments on the text.

References

Baars, J. W. M., Genzel, R., Pauliny-Toth, I. I. K., & Witzel, A. 1977, A&A, 61, 99
Brentjens, M. A., & de Bruyn, A. G. 2005, A&A, 441, 1217
Conway, R. G., Garrington, S. T., Perley, R. A., & Biretta, J. A. 1993, A&A, 267, 347
Davis, R. J., Muxlow, T. W. B., & Conway, R. G. 1985, Nature, 318, 343
Jester, S., Röser, H. -J., Meisenheimer, K., & Perley, R. 2005, A&A, 431, 477
Martel, A. R., Ford, H. C., Tran, H D., et al. 2003, AJ, 125, 2964
Perley, R. A., & Butler, B.J. 2013a, ApJS, 204, 19
Perley, R.A., & Butler, B. J. 2013b, ApJS, 206, 16
Perley, R. A., & Butler, B. J. 2017, ApJS, submitted
Schmidt, M. 1963, Nature, 197, 1040
van der Laan, H. 1966, Nature, 211, 1131
Zavala, R. T., & Taylor, G. B. 2005, ApJ, 626, L73